Surface Behavior of *N*-Dodecylimidazole at Air/Water Interfaces

Javier Rodriguez and Daniel Laria*

Departamento de Química Inorgánica, Analítica y Química-Física e INQUIMAE, Facultad de Ciencias Exactas y Naturales, Universidad de Buenos Aires, Ciudad Universitaria, Pabellón II, 1428, Buenos Aires, Argentina, and Unidad Actividad Química, Comisión Nacional de Energía Atómica, Avenida Libertador 8250, 1429, Buenos Aires, Argentina

Received: August 7, 2006; In Final Form: October 14, 2006

Using molecular dynamics techniques, we investigate surface states of the surfactant *N*-dodecylimidazole (DIm) in its basic and acid forms adsorbed at the water/air interface. Two different surface coverages were examined: an infinitely diluted detergent and a saturated monolayer. Spatial and orientational correlations of the surfactants and the aqueous substrate are presented. At large surface coverages, DIm presents two solvation states with well differentiated structural and dynamical characteristics. Solvation of the protonated surfactant becomes unstable at large concentrations, while the relative stability of the surface states of *N*-dodecylimidazolium ($DImH^+$) with respect to bulk states increases at infinite dilution. The surface acidic behavior of $DImH^+$ was investigated using a multistate empirical valence bond Hamiltonian model. Our simulation results suggest that the acidic characteristics of DIm are enhanced at the surface. The differences are rationalized in terms of the distinctive features in the overall solvation structure of the reactive complex.

I. Introduction

In this paper, we examine the surfactant characteristics of *N*-dodecylimidazole (DIm) and *N*-dodecylimidazolium ($DImH^+$; see Figure 1) adsorbed at water/air interfaces. These environments are inhomogeneous at the nanometer scale and can host a large variety of chemical reactions.[1−3] Contrasted to what is perceived in isotropic phases, equilibrium and dynamical characteristics of surface reactions normally exhibit profound modifications. From a microscopic perspective, the origins of these modifications can normally be traced back to the large imbalances in the prevailing intermolecular force fields. Under these circumstances, it is not unusual to find large concentration fluctuations,[4] modifications in the intramolecular hydrogen bond (HB) connectivity,[5] changes in the local polarity, and alterations in the characteristic time scales describing microscopic relaxation processes.[6] These phenomena, in turn, get translated into displacements of chemical equilibria,[7] local changes in pH,[8] and modifications in the rates[9] of surface reactions, to list just a few examples of experimental evidence.

The analysis of surface states of DIm is akin to a couple of recent studies performed on a variety of room-temperature ionic liquids based on *N*,*N*′-dialkylimidazolium cations. Using sum-frequency vibrational spectroscopy techniques, Fitchett and Conboy[10] have analyzed the adsorption of these ionic liquids at SiO_2 surfaces. In a related context, Bowers et al.[11] have also examined the adsorption of similar ionic fluids at water/air interfaces, focusing on the prevailing structures of the adsorbed monolayers. Results from their neutron scattering experiments show a rich variety of structures, which seem to be strongly dependent on the surface activity of the particular anion considered (tetrafluoroborate, iodide, or chloride). From a biological point of view, the detergency of DIm, combined with its acid/basic behavior, seems to play a key role controlling its action as a cytotoxic agent. In this context, DIm is usually

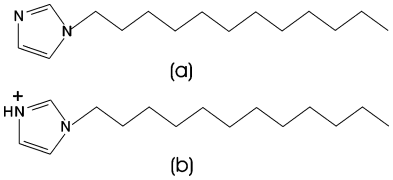

Figure 1. (a) DIm. (b) $DImH^+$.

referred to as a "lysosomotropic" agent,[12] a molecule that is able to permeate through the lysosomal membrane becoming protonated in the low pH environment that prevails in the interior of the vesicle. Furthermore, it has been suggested that the accumulated $DImH^+$ acquires surfactant characteristics, promoting the structural destabilization of the lysosome membrane. This action, in turn, would lead to the cell death, as the lysosome contents come in contact with the cytoplasm.[13,14] More recently, new experimental results have clashed with the latter description, which still awaits further elucidation.[15,16]

The previous considerations have underlined the relevance of the main objective of this paper, where we will present results from molecular dynamics experiments describing monolayers of DIm adsorbed at water/air interfaces at different surface coverage regimes. The implemented model is based, to a large extent, on previous simulation studies of acid/base equilibria of imidazole (Im) in bulk water.[17,18] Following these works, we also analyze different and important aspects dealing with the protonation of the surfactant at the surface. The key aspect that we examine is whether the interfacial acidity of DIm is enhanced or diminished with respect to what is observed in bulk. In a wider context, this problem is akin to the characterization of the surface activity of aqueous protons, a subject that has received considerable attention in recent times.[19−21]

Results from second harmonic generation experiments indicate that acid/base equilibria at aqueous surfaces can be shifted in either direction, depending on the overall electrostatic characteristics of the reactant and product states.[22,23] With the

* Corresponding author. E-mail: dhlaria@cnea.gov.ar.

10.1021/jp0650883 CCC: $37.00
Published on Web 12/05/2006

exception of ref 21, we are not aware of previous studies in which the characteristics of acid/base equilibria at air/water interfaces were investigated from a microscopic perspective.

The organization of the present work is as follows: in the next section, we present an overview of the model and the simulation procedure. The central part of the paper (section III) is devoted to the simulation results and includes a description of the surface solvation structures of DIm. In section IV, we examine surface states for $DImH^+$ and its acid/base equilibrium at the surface. The concluding remarks are summarized in the last section.

II. Model and Simulation Procedure

A. Dodecylimidazole and Water. The simulation runs were performed on systems containing different amounts N_s of DIm and $DImH^+$ adsorbed at the water/air interface of a slab composed of $N_w = 341$ water molecules. Three different surfactant coverages were considered: (i) first, we examined systems with a surface coverage close to the full monolayer (with an area per surfactant molecule, $\rho_s^{-1} \sim 30$ Å^2), (ii) second, we analyzed the adsorption of a single surfactant at infinite dilution, and (iii) finally, a few test runs at an intermediate density of $\rho_s^{-1} \sim 60$ Å^2 were also performed. The water sample was obtained from a previously equilibrated periodic system of linear dimensions 20.0 Å × 20.0 Å × 25.83 Å in which periodic boundary conditions were suppressed along the direction of the longest axis of the simulation box (hereafter referred to as the *z*-axis). For the more diluted runs and in order to sample spatial correlations at the surface of longer wavelengths, the number of water molecules was taken up to $N_w = 648$, while the box dimensions were set at 28.06 Å × 28.06 Å × 24.95 Å. The initial configuration of the interfacial environment was constructed by distributing the surfactant molecules with their imidazole groups lying in the vicinity of one of the slab's free interfaces. The intramolecular configurations of the hydrophobic tails corresponded, in this case, to fully trans conformers, while their head-to-tail vectors were oriented perpendicular to the plane of the interface.

Water molecules were modeled using the flexible TIP3P mean field model.[24] A flexible model Hamiltonian was also adopted for the surfactant; the intramolecular modes included stretching, bending, and dihedral and nonbonding contributions. Using the united atom description for the CH_2 and CH_3 groups, we found that the surfactant tails comprised a total of 12 sites. Inter- and intramolecular potentials involving these groups were taken from the GROMACS force field.[25] Intramolecular and intermolecular interactions pertaining to the imidazole ring sites were modeled with full atomistic detail. The functional forms of the intra- and intermolecular Hamiltonian involving these sites of the surfactants were taken from previous works by Čuma et al.[17,18]

Long ranged Coulomb interactions were treated using Ewald summation techniques by implementing a particle mesh procedure adapted for slab geometries.[26] Since the simulated system has a net charge, the presence of a uniform, neutralizing background was assumed. The dynamical trajectories corresponded to microcanonical runs at temperatures close to $T \approx 298$ K. In this temperature regime, the slabs presented stable structures with negligible evaporation. Production runs were preceded by thermalization periods of 500 ps, in which only the surfactant tails were allowed to move at $T \sim 700$ K. From then on, the systems were gradually cooled down to ambient conditions during subsequent time intervals of 250 ps. Meaningful statistics were collected along equilibrium trajectories of ~2−5 ns.

B. Dodecylimidazolium. For the simulation experiments in which the behavior of $DImH^+$ was analyzed, we resorted to an extended empirical valence bond (EVB) scheme. This approach has been extensively exploited in the past[27−30] to analyze chemical reactivity in a variety of environments, including the related case of imidazolium in bulk water.[17,18,31] The basic ingredient of the scheme involves the construction of an EVB Hamiltonian of the type

$$\hat{\mathbf{H}}_{\mathrm{EVB}}(\{\mathbf{R}\}) = \sum_{ij} |\phi_i\rangle h_{ij}(\{\mathbf{R}\})\langle\phi_j| \tag{1}$$

In the previous equation, $|\phi_i\rangle$ represents a basis set of diabatic valence bond (VB) states denoting different spatial localizations of the excess proton. The basis set was constructed considering the two types of diabatic states illustrated in the following acid/base equilibrium in solution:

$$DImH^+ + H_2O \rightleftharpoons DIm + H_3O^+ \tag{2}$$

The first type, $|DImH^+\rangle$ (reactant side), designates proton localization at the imidazole ring. The second class (product side) includes the set of states, $\{|H_3O^+\rangle\}$, in which the surfactant is in its basic form and the excess proton localizes in a nearby water molecule. At each step of the simulation, the construction of the EVB Hamiltonian was guided by the pattern of a HB network started at the instantaneous position of the excess charge. Typically for interfacial protons, approximately eight diabatic states were included in the EVB Hamiltonian. This number did not change considerably (up to a total of ~10) for a few test runs that we also performed in fully periodic systems.

The dynamics of the classical nuclei were generated from the Born−Oppenheimer potential energy surface obtained from $\epsilon_0(\{\mathbf{R}\})$, the lowest eigenvalue of the EVB Hamiltonian:

$$\hat{\mathbf{H}}_{\mathrm{EVB}}|\psi_0\rangle = \epsilon_0(\{\mathbf{R}\})|\psi_0\rangle \tag{3}$$

where $|\psi_0\rangle$ is the corresponding eigenstate. Expressed in terms of the diabatic states, the ground state can be written as

$$|\psi_0\rangle = \sum_i c_i|\phi_i\rangle \tag{4}$$

which leads to the following expression for $\epsilon_0(\{\mathbf{R}\})$:

$$\epsilon_0(\{\mathbf{R}\}) = \sum_{ij} c_i c_j h_{ij}(\{\mathbf{R}\}) \tag{5}$$

Invoking Hellmann−Feynman's theorem,[32] Newton's equation of motion for classical nuclei of mass M_k can be readily obtained as

$$M_k \frac{\mathrm{d}^2\mathbf{R}_k}{\mathrm{d}t^2} = -\sum_{ij} c_i c_j \nabla_{\mathbf{R}_k} h_{ij}(\{\mathbf{R}\}) \tag{6}$$

Full details of the simulation procedure can be found in refs 17, 18, 26, and 27.

Čuma et al.[17,18] have extensively analyzed the acid characteristics of the imidazolium (ImH^+) cation in bulk water and have derived appropriate parametrizations for the different matrix elements $h_{ij}(\{\mathbf{R}\})$ in terms of the nuclei coordinates. Given the similarities between the reported acidic behavior of DIm ($pK_a = 7.4$) and that of Im ($pK_a = 6.97$),[33] only two minor changes in the original parametrization of Čuma and co-workers were operated: (i) we supplemented the diagonal matrix elements with additional Lennard-Jones contributions arising

from the interactions involving sites in the hydrocarbon chain, and (ii) for the protonated imidazole ring, we found it also convenient to replace the non-dissociative harmonic representation of the $N-H^+$ stretching mode, with a dissociative Morse interaction of the type[31]

$$V_{NH^+}(r) = D_e[1 - \exp[-\lambda(r - r_0)]]^2 \quad (7)$$

with $r = |\mathbf{r}_N - \mathbf{r}_{H^+}|$, $D_e = 144.3$ kcal mol^{-1}, $\lambda = 2.77$ Å^{-1}, and $r_0 = 1.03$ Å. Results from this new parametrization practically coincide with those reported by Cuma et al. for energy profiles describing the deprotonation of ImH^+ in small water clusters.[18]

III. Surfactant Behavior of DIm

In this section, we will examine the structural characteristics of an adsorbed monolayer of DIm at a water/air interface, close to surface saturation. Unfortunately, we know of no previous study where surface coverages in this regime are reported. In principle, reasonable estimates could be obtained from a previous study by Bowers et al.[11] in which the surface behaviors of related room-temperature ionic liquids involving *N*-alkyl-*N*-methylimidazolium salts were investigated. More specifically, Bowers et al. found that, depending on the particular anion considered, the adsorbed monolayers typically saturate at $\rho_s^{-1} \simeq 60-100$ Å^2. Although the structural characteristics of the cations of these ionic fluids are similar to those of DIm, it is important to keep in mind that the presence of charged species (and more importantly, surface active anions such as iodides[4]) might preclude establishing a straightforward correspondence between the observed values of ρ_s for surface ionic liquids and the present case.

As a practical solution, we determined the surface coverage from a series of preliminary runs, during which we analyzed the structural stability of interfaces containing increasing numbers of surfactant molecules. First, we analyzed adsorption at intermediate coverages, that is, at $\rho_s^{-1} \simeq 60$ Å^2 ($N_s = 6$). Under these circumstances, the prevailing surfactant structures could be pictured as a single "patch" of headgroups with their hydrophobic tails mostly parallel to the interface, pointing radially outward from the clustered headgroups. The direct inspection of a large number of these structures showed that approximately half of the water molecules at the interface were involved in the solvation of the headgroups, while the rest were in contact with the adsorbed tail groups. Keeping this qualitative picture in mind, we finally adopted $\rho_s^{-1} = 30.8$ Å^2 ($N_s = 13$) for a system close to saturation, which represents a lower bound value below which several surfactants begin to lose contact with the substrate and eventually evaporate.

Figure 2 displays a snapshot of the self-assembled structure of adsorbed surfactants. At a first glance, we believe two features are worth mentioning: (i) a large contact area between the Im rings and the water substrate and (ii) a rather uniform overall tilt for the hydrophobic tails. More quantitative information about these structural features can be acquired from the density profiles that are shown in Figure 3. In particular, we present plots for

$$\rho_w(z) = \frac{1}{A}\langle\sum_{i=1}^{N_w}\delta(Z_i - Z_{CM} - z)\rangle \quad (8)$$

where $\rho_w(z)\,dz$ represents the average number of water molecules per unit of area A whose centers of mass lie between z and $z + dz$. In the previous equation, $\langle ... \rangle$ denotes an equilibrium

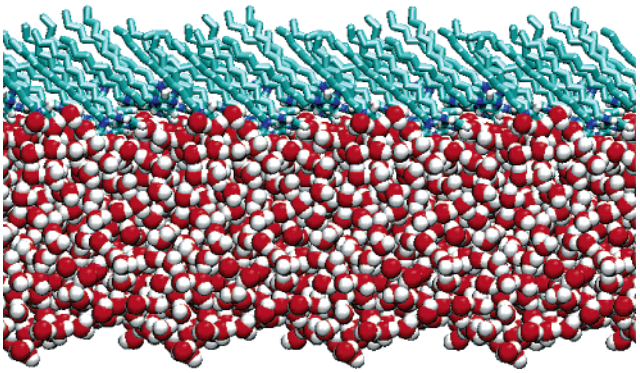

Figure 2. Snapshot of a typical configuration of DIm adsorbed at an air/water interface close to surface saturation. For clarity purposes, the system has been replicated three times along a direction parallel to the interface.

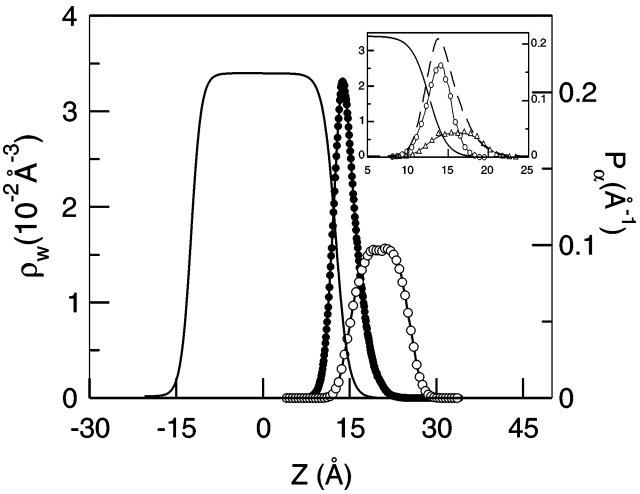

Figure 3. Local water density (thick solid line, left axis) and normalized probability densities for different head (black circles) and tail (open circles) sites. In the inset, contributions to the total head distribution (dashed lines) from solvation states $\mathscr{A}$ and $\mathscr{B}$ are shown with circles and triangles, respectively.

ensemble average, while Z_i and Z_{CM} represent the z coordinates of the ith water molecule and the center of mass of the slab, respectively.

Both interfaces can be reasonably well approximated using the standard mean field formula:

$$\rho_w(z) \sim \frac{\rho_b}{2}\left[1 - \tanh\frac{z - \bar{z}_w}{\Delta z_w}\right] \quad (9)$$

The overall profile is rather symmetric with respect to Z_{CM}: $\bar{z}_w = -12.50$ Å and $\bar{z}_w = 12.61$ Å for the bare and coated surfaces, respectively. In addition, the presence of surfactant induces an ~20% widening of the nearby interface: $\Delta z_w = 2.2$ Å (right) versus $\Delta z_w = 1.8$ Å (left). Figure 3 also includes results for spatial correlations involving headgroups and hydrophobic tails of the type

$$P_\alpha(z) = \langle\sum_{i=1}^{N_s}\delta(z_i^\alpha - Z_{CM} - z)\rangle \quad (10)$$

where z_i^α represents the site α of the ith surfactant. For the first case, we included correlations of the z coordinates of all imidazole ring sites while, for the tails, we included correlations of the z coordinates of all tail groups. The headgroup profile exhibits a Gaussian-like profile, centered at $\bar{z} = 14.48$ Å, with

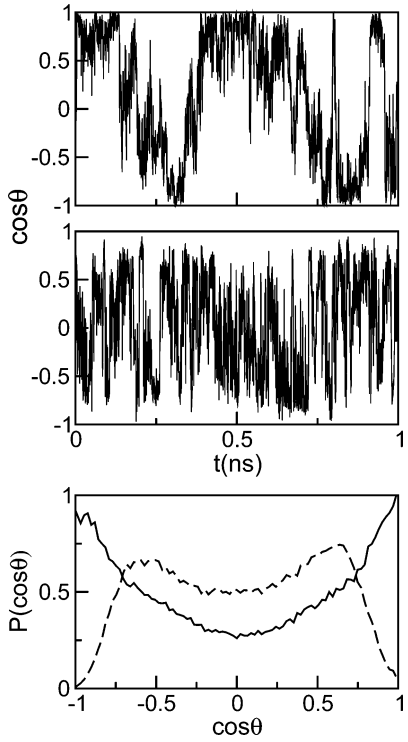

Figure 4. Time evolutions of cos θ (see text) for solvation states $\mathscr{A}$ (top panel) and $\mathscr{B}$ (middle panel). The bottom panel shows probability distributions for states $\mathscr{A}$ (solid line) and $\mathscr{B}$ (dashed line).

a dispersion comparable to the width of the interface $\Delta z = 2.18$ Å. On the other hand, the overall average position of the hydrophobic chain distribution is centered somewhat outward from the position of the heads, $\langle z \rangle = 20.26$ Å, and presents a wider dispersion $\langle (\delta z)^2 \rangle^{1/2} = \langle (z - \langle z \rangle)^2 \rangle^{1/2} = 3.39$ Å.

A more detailed analysis of the head distribution shows that the curve is in fact the result of two well resolved subdistributions describing different solvation environments (hereafter referred to as $\mathscr{A}$ and $\mathscr{B}$ surface states). The gross features of these states can be easily identified in terms of the localization of the headgroups within the interface, the headgroups solvated in states of type $\mathscr{A}$ being embedded more in the aqueous phase than those in states of type $\mathscr{B}$ (see inset in Figure 3). The integral of the curve shown in the inset shows that ~40% of the headgroups are solvated in $\mathscr{A}$ environments. Moreover, in the course of trajectory (~2−5 ns), we typically encountered very few events where the headgroups would interchange their solvation status, suggesting that these transitions require slow fluctuations characterized by time scales comparable to, or even longer than, the length of the simulation experiments.

We also analyzed orientational correlations of the surfactants. For headgroups, a natural variable to monitor is $\cos \theta_i = \hat{\mathbf{z}} \cdot \hat{\mathbf{z}}'_i$, where $\hat{\mathbf{z}}'_i$ represents a unit vector along the direction perpendicular to the imidazole plane of the *i*th headgroup. In the top and middle panels of Figure 4, we present results for the time evolutions of cos θ_i corresponding to two tagged molecules exhibiting solvation states $\mathscr{A}$ and $\mathscr{B}$. The curve for type $\mathscr{A}$ can be pictured as a sequence of episodes, during which cos θ_i remains close to ±1, a fact that is accordant to the above-mentioned observation of large contact areas between the aqueous substrate and the DIm ring. These stable solvation stages are separated by transitions, during which the face of the DIm ring in contact with water flips over. Moreover, these transitions seem to be triggered by a previous detachment from the substrate before "landing back" on the interface (see sequence in Figure 5). The direct comparison between the top

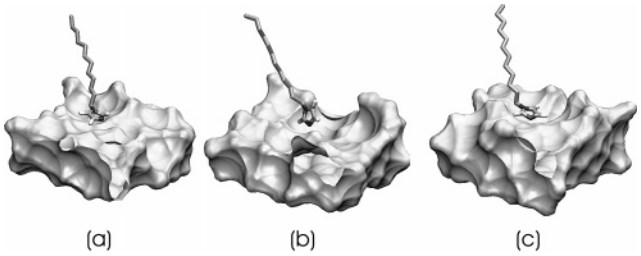

Figure 5. Snapshots for the surface flipping of DIm at high coverages. The configurations correspond to the trajectory shown in the top panel of Figure 4 at (a) $t = 0.1$ ps, (b) $t = 0.25$ ps, and (c) $t = 0.6$ ps. For clarity purposes, the rest of the surfactants are not shown.

($\mathscr{A}$) and middle ($\mathscr{B}$) panels of Figure 4 shows that, for the former states, not only does cos θ_i remain much closer to ±1, but also the individual rates of flipping transitions seem to be smaller. From a qualitative point of view, a corroboration of these observations can be obtained from the corresponding maxima of the symmetric distributions shown in the bottom panel of Figure 4:

$$P[\cos \theta] = \langle \delta[\cos \theta_i - \cos \theta] \rangle \tag{11}$$

Note that, for states $\mathscr{A}$, the maxima are located at cos $\theta = \pm 1$ while for states of type $\mathscr{B}$ the maxima are shifted to cos $\theta \sim \pm 0.6$. We analyzed the overall tilt distributions (not shown) described in terms of

$$\cos \alpha = \frac{z_{C_{12}} - z_{C_1}}{|\mathbf{r}_{C_{12}} - \mathbf{r}_{C_1}|} \tag{12}$$

where C_i denotes the *i*th carbon in the hydrophobic chain. Both distributions were practically identical, with average values $\langle \cos \alpha \rangle = 0.74$.

IV. Surface States of $DImH^+$

A. Solvation Structures. We now turn to the analysis of the surface behavior of $DImH^+$. To that end, several statistically uncorrelated configurations of the system described in the previous section were used as initial conditions of a second series of simulation runs, in which one randomly chosen DIm was replaced by $DImH^+$. A total of 10 different runs were analyzed. The top panel of Figure 6 shows a typical time evolution of z_{Im}, that is, the *z* coordinate of the center of the imidazole ring (green line). It is clear that the stability of $DImH^+$ at the interface is drastically modified; the protonated surfactant diffuses into the bulk phase in a barrierless fashion and becomes fully solvated in the course of a few picoseconds (see also the top panels of Figure 7). This new result reveals differences at a qualitative level between the surface activities of protonated $DImH^+$ and those of its conjugated basic form DIm that we will consider in the next paragraphs.

In order to examine the reasons for the destabilization of surface states of $DImH^+$ in the presence of a full monolayer of DIm, we moved to the examination of a simpler case, that is, its adsorption at infinite surface dilution. The time evolution of z_{Im} along a typical run under these conditions is also shown in the top panel of Figure 6 (black line). Note that, in the absence of DIm, the surface stability of $DImH^+$ is dramatically enhanced. In any case, the trajectory still shows a fairly prolongated episode (220 ps $\lesssim t \lesssim$ 380 ps), during which the single head plunges into the bulk deeper than the width of the interface (see also bottom panels of Figure 7). More interestingly, we found evidence that the onsets of these episodes seem to be

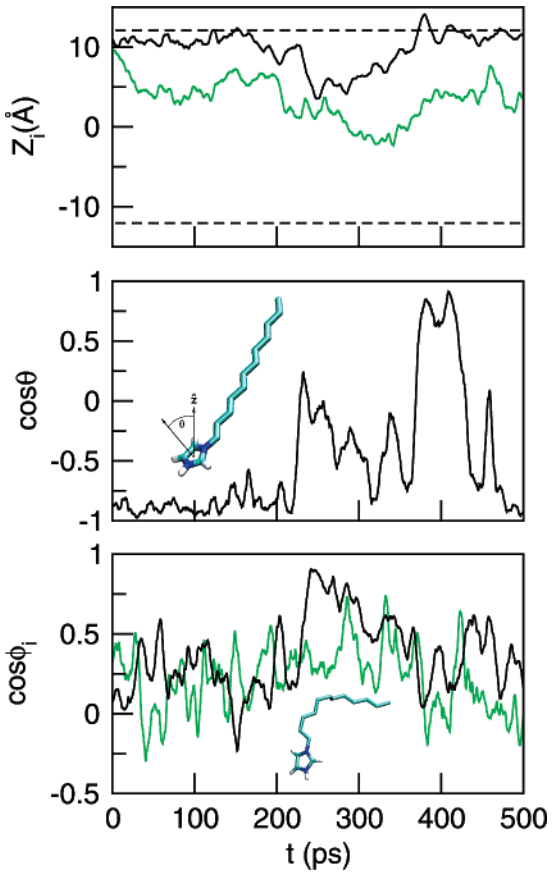

Figure 6. Top panel: time evolutions of z_{DIm} for $DImH^+$ at full coverage (green line) and at infinite dilution (black line). The dashed lines correspond to the position of the interfaces. Middle panel: time evolution of cos θ at infinite dilution. Bottom panel: time evolutions of cos ϕ_i (see text) at infinite dilution [$i = 1$ (black line); $i = 2$ (green line)].

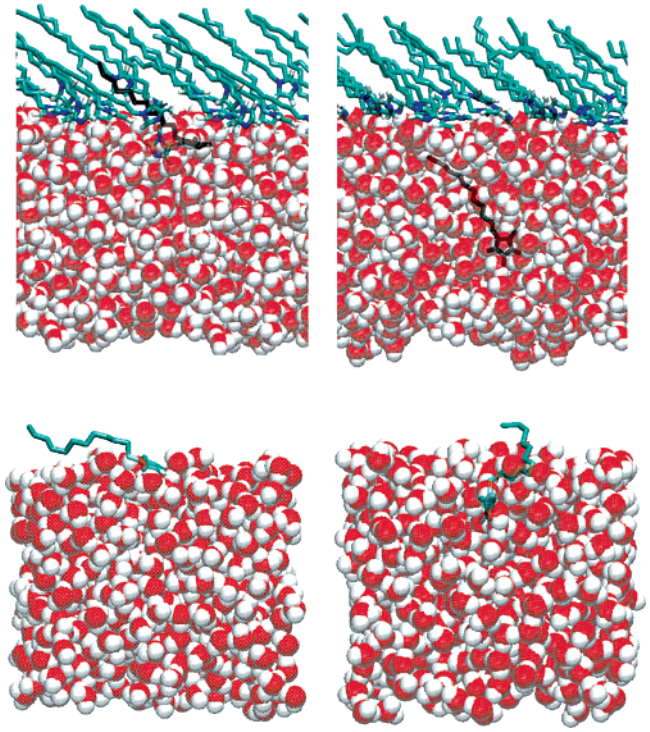

Figure 7. Snapshots of configurations of $DImH^+$ taken from the trajectories shown in Figure 6. Top panels, full coverage; bottom panels, infinite dilution. The left- and right-hand side panels correspond to $t = 0$ ps and $t = 300$ ps, respectively.

triggered by the temporal coincidence of two, and in principle uncorrelated, events. The first one involves the partial protonation of the Im ring, leading to a configuration in which the imidazolium plane becomes perpendicular to the interface. We tend to believe that this geometrical arrangement would facilitate the gradual incorporation of the headgroup into the bulk phase, driven by the simultaneous solvation of both faces of the ring. In addition, the mechanism of penetration of the surfactant into the bulk phase would also require the previous desorption of a sizable portion of the hydrocarbonate chain from the surface.

The examination of time evolutions of the set of relevant degrees of freedom shown in the middle and lower panels of Figure 6 is instructive to corroborate the previous assertions. In the middle panel, we show results for the time evolution of cos θ. The sudden rise from ~ -1 up to ~ 0.2 at $t \sim 220$ ps clearly correlates with the onset of the penetration into the bulk. The lower panel includes results for two angles describing tilts of two different portions of the hydrocarbon chain, namely,

$$\cos\phi_1 = \frac{z_{C_5} - z_{Im}}{|\mathbf{r}_{C_5} - \mathbf{r}_{Im}|} \quad \text{and} \quad \cos\phi_2 = \frac{z_{C_{12}} - z_{C_6}}{|\mathbf{r}_{C_{12}} - \mathbf{r}_{C_6}|} \quad (13)$$

Again, the immersion episode coincides with modifications in the overall tilts of the closest and farthest, with respect to the headgroup, segments of the tail. While the latter gets into the bulk by adopting a perpendicular orientation with respect to the interface ($\cos\phi_1 \sim 0.9$), the more distant portion of the tail retains its original, mostly parallel alignment and remains at the surface, preventing the full solvation of the surfactant. Note that the overall picture that emerges from these observations provides arguments to rationalize the instabilities of surface states and the subsequent full bulk solvation of $DImH^+$ in the presence of a monolayer of DIm close to surface saturation. Under these conditions, fluctuations due to packing effects between surfactants would provoke more frequent detachments of the $DImH^+$ ring because of competition for surface contact with the rest of the headgroups and a more uniform overall tilt of the hydrophobic tails. Both effects, in turn, would facilitate the pathway of the charged surfactant into the bulk, with practically no free energy barrier.

B. Acid/Base Equilibrium for $DImH^+$. The final aspect that we will examine deals with the acid/base characteristics of DIm. More specifically, our aim was to assess possible changes in its surface acidity, compared to the one observed in bulk. Perhaps the most direct route to analyze these differences would require the evaluation of a thermodynamic cycle in which free energy differences between reactant and product states are computed in both environments. These calculations should be complemented with estimates of the reversible work required to transfer reactant and product species from the bulk to the surface. Although the basic ideas underlying this cyclic process are conceptually well established, their practical evaluation often presents serious drawbacks, most notably, those pertaining to the identification of an appropriate reaction coordinate joining reactant and product states.[34]

In the present work, our objective was restricted to estimating the relative stabilities of reactant and product states at the interface and in bulk water. To do so, we closely followed the procedure described by Voth et al.[18,35] in their analysis of the ImH^+ and other acids in bulk water. Briefly, a reaction coordinate based on the spatial localization of the excess proton was postulated, and a free energy profile along this degree of freedom was constructed using standard non-Boltzmann sam-

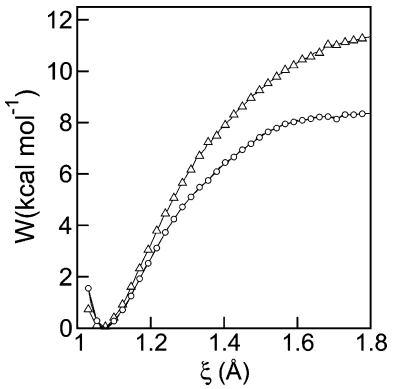

Figure 8. Free energy profiles for the proton detachment from $DImH^+$ for surface (circles) and bulk (triangles) solvation states.

pling techniques. In our case, the reaction coordinate ξ was chosen to be

$$\xi = |\bar{\mathbf{r}}_p - \mathbf{r}_N| \tag{14}$$

In the previous equation, $\mathbf{r}_N$ denotes the position of the protonable N site in the imidazole ring, and $\bar{\mathbf{r}}_p$ represents a weighted sum of proton localizations in different diabatic states, namely,

$$\bar{\mathbf{r}}_p = \sum_i c_i^2 \, \bar{\mathbf{r}}_i \tag{15}$$

For the single VB state of type $|DImH^+\rangle$, $\bar{\mathbf{r}}_i = \mathbf{r}_{H^+}$; for the set of $\{|H_3O^+\rangle\}$ states, $\bar{\mathbf{r}}_i$ coincides with the position of the oxygen atom in each tagged H_3O^+ hydronium state. This reaction coordinate is slightly different, although in principle, it is equivalent to that adopted by Čuma et al.[18]

The trajectory shown in the top panel of Figure 6 shows that the solvation of the headgroup of the isolated $DImH^+$ could be regarded as mostly interfacial. However, we mentioned that spontaneous episodes of bulk solvation also occur in the time scale of our simulations. To filter out the latter effects and concentrate on surface solvation, we found it convenient to supplement the EVB Hamiltonian with an extra confining potential term V_{cf} acting on the center of mass of the Im ring of the type

$$V_{cf} = \frac{k_{cf}}{2}(|z_{Im} - Z_{CM}| - \bar{z})^2 \tag{16}$$

With the restoring force constant k_{cf} set to 50 kcal mol^{-1} Å^{-2}, we succeeded in restricting the sampling to a rectangular slab of roughly 3 Å in width, centered at $\bar{z} \sim 13$ Å. This procedure has been frequently implemented in the past to analyze surface states of many solutes.[36−39]

In Figure 8, we present results for the free energy profile $W(\xi)$, namely,

$$e^{-\beta W(\xi')} \propto \langle \delta(\xi - \xi') \rangle \tag{17}$$

where β^{-1} is the Boltzmann constant times the temperature. The curves were obtained by implementing a standard umbrella sampling procedure[40,41] with a bias harmonic potential applied on the reaction coordinate. For the sampling interval displayed in Figure 8, seven windows were required with umbrella force constants of the order of $k_{bias} \sim 10^2$ kcal mol^{-1} Å^{-2}.

Two features of Figure 8 are worth mentioning: (i) both curves show single minima at $\xi = 1.08$ Å, corresponding to the stable reactant state $DImH^+ + [H_2O]_{N_w}$; (ii) at larger values, there are no second minima, and both curves seem to level off at practically plateau values, the one for the surface transfer being ∼3 kcal mol^{-1} higher than that for bulk. Results in Figure 8 do not surpass $\xi_{max} = 1.8$ Å; beyond this value, simulation experiments started with equivalent initial conditions yield large inconsistencies in the apparently converged histogram profiles that persist, even after collecting statistics for time spans of several nanoseconds.

To unveil the origins of the lack of a uniform convergence, we examined many configurations for ξ close to ξ_{max}. Expressed in terms of the typical magnitudes of the two largest expansion coefficients shown in eq 4 ($c_{|DImH^+\rangle}^2 \sim 0.15$; $c_{|H_3O^+\rangle}^2 \sim 0.75$), the configurations corresponded to the product states: a DIm plus a hydronium state localized in a neighbor water. Under these circumstances, we tend to believe that the lack of uniform convergence would indicate that the umbrella procedure failed to capture the manifold of relevant pathways through which the actual deprotonation process evolved, beyond the first elemental transfer step. Note that, following this first step, the mechanism of proton detachment may be rather complex involving not only standard, that is, Stokes-like, diffusion of the H_3O^+ acceptor from the DIm, but also a subsequent proton transfer to a second water molecule lying in an outer shell, operated via the Grotthus mechanism. Moreover, we recall that, for the simpler symmetric proton-transfer processes, namely,

$$H_3O^+ + H_2O \rightleftharpoons H_2O + H_3O^+ \tag{18}$$

the time limiting step and the actual reaction coordinate are to be found in subtle modifications in the local structure of HBs in the second and possibly third solvation shells of the reactants.[42] Consequently, if similar characteristics persist in surface proton-transfer processes, it should not come as a surprise that the umbrella procedure may become inefficient to conduct the sampling across all relevant portions of the phase space. A more detailed analysis of the reaction pathways was well beyond the scope of this work, so we did not proceed with any further examinations along these directions.

Anyhow, we believe that the results depicted in Figure 8 still remain physically sound and that, on the basis of the observed free energy differences $\delta F(\xi_{max}) \sim 3$ kcal mol^{-1}, one can conclude that the acid characteristics of $DImH^+$ are enhanced at the surface. Before closing this section and in order to obtain some clues concerning the reasons for the surface acid enhancement, we performed a few exploratory tests focused on the solvation structures of the reactant $DImH^+ + [H_2O]_{N_w}$ moiety in bulk and surface environments. We started by considering some relevant site distances involving the $NH^+\cdots O$ group. In all cases, we found no significant modifications (typically $\lesssim$0.05 Å) in the geometrical arrangement of the complex ($d_{NH} = 1.06$ Å, $d_{NO} = 2.56$ Å, $d_{HO} = 1.52$ Å) that would allow one to foresee the observed changes in the free energies. We then moved further outward to the consideration of spatial correlations involving the closest solvation shell of the water proton acceptor. In Figure 9, we present results for pair correlation functions (left axis) of the type

$$\rho_\gamma g_{\alpha\gamma}(r) = \frac{1}{4\pi r^2} \langle \sum_{i=1}^{N_w - 1} \delta(|\mathbf{r}_\alpha - \mathbf{r}_\gamma^i| - r) \rangle \tag{19}$$

where the first index denotes sites in the tagged water molecule and the second one refers to sites in the rest of the water sample. For completeness, Figure 9 also includes results for cumulative integrals (right axis).[43] The top and bottom panels include three

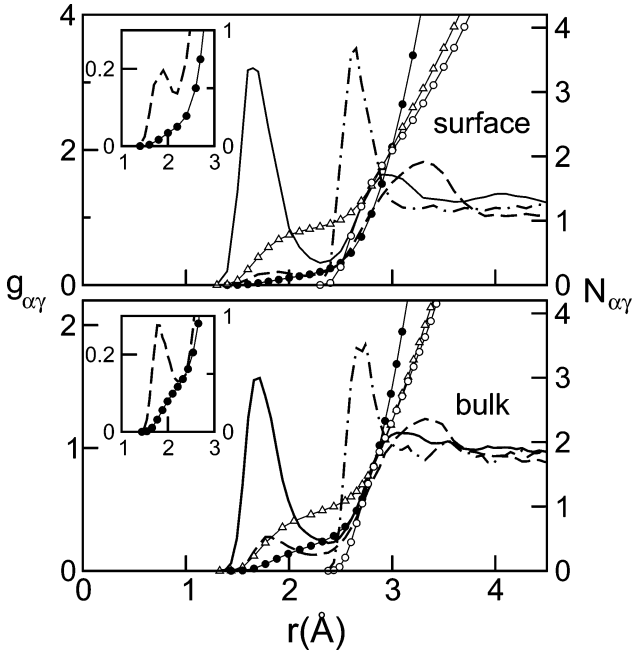

Figure 9. Pair correlation functions (left axis) and cumulative integrals (right axis) for the solvation of the proton acceptor water. O−O, dotted-dashed lines and open circles; H−O, solid line and triangles; O−H, dashed lines and black circles.

pairs of curves corresponding to O−O, O−H, and H−O correlations; the last two sets allow for the discrimination of the connectivity of the tagged water in terms of its HB donor and acceptor characters. Regardless of the particular environment considered, the overall shape and the positions of the main peaks of $g_{OO}(r)$ are rather similar and so are the ones for $g_{HO}(r)$, centered at the $r = 1.65$ Å and including one oxygen atom. The latter observation would confirm the HB dual-donor character of the tagged water molecule. Distinctive features do appear as one analyzes the acceptor characters (g_{OH} curves). Note that, compared to bulk results, the peak for surface environments shifts from 1.82 Å up to 1.9 Å, while its area drops from 0.44 down to 0.16 (see Figure 9 insets). These results would suggest that, in surface environments, the acceptor characteristics of the tagged water with respect to the rest of the solvent are drastically deterred. In passing, we mention that a distinctive characteristic of the solvation structure of the hydronium in water is the absence of HB of $H_3O^+\cdots$HOH type. Consequently, the original HB connectivity, in turn, would facilitate the transfer of the excess proton without involving major rearrangements of the environment to accommodate a newly formed H_3O^+.

V. Concluding Remarks

The molecular dynamics results presented in this paper show interesting features pertaining to the detergency and the chemical reactivity of DIm adsorbed at water/air interfaces. In particular, at large surface coverages, we found that the solvation structure of DIm can be pictured as composed by two types of states, with well differentiated structural and dynamical characteristics. Surfactants solvated in embedded states of type $\mathscr{A}$ lie deeper inside the aqueous substrate, and their overall dynamics looks slower than that for "more external" states of type $\mathscr{B}$. In the nanosecond time scale, the relevant dynamics that we observed was mainly the one related to flipping of the planes of the headgroups, which are operated via a complete detachment of the surfactants from the substrate.

The original balance between bulk and surface solvation forces disappears when a neutral surfactant is replaced by a protonated one. As a result, the charged surfactant is dragged into the condensed phase almost immediately. Reduction in the overall surfactant density modifies this behavior, and at infinite dilution, the protonated surfactant recovers its former surface stability. Still, the molecular dynamics trajectories include periods, in the time scale of a few hundreds of picoseconds, during which the headgroup is partially incorporated inside the bulk, being "anchored" at the interface by the distal part of the hydrophobic tail. The overall picture that emerges from our simulations suggests that it is the adsorption of the tail segment that remains in contact with the surface, the key process that prevents the complete solvation of the surfactant. As such, our results would indicate that the dynamical pathways joining surface and bulk solvation states for the protonated species are controlled to a non-negligible extent by fluctuations in the overall structure and orientation of the hydrophobic tails.

We also analyzed the acid characteristics of the surfactant at the interface. Although not completely conclusive, the free energy profile obtained for the detachment of the proton from the $DImH^+$ into a surface water shows a larger propensity for losing the proton. In a related context, these results are in accordance with data from second harmonic generation experiments performed on surfactants with quaternary nitrogens, such as $CH_3(CH_2)_{21}NH_3^+$, which also show acid enhancements at the surface.[23] Expressed in terms of decreasing degrees of solvation, the trend would indicate that the acidic characteristics of $DImH^+$ gradually diminish as we move from bulk to surface environments. Our simulation results also suggest that a plausible reason in accounting for the changes in the acidic behavior might be found in a more favorable surface solvation of the proton-receptor water at the reactant state, whose HB connectivity looks similar to the one exhibited by the hydronium at the product state. This scenario would precondition the charge-transfer process at a lesser energy cost originated in the reorganization of the solvation environment.

Still, many open questions remain to be answered concerning the characteristics of proton-transfer processes in inhomogeneous media, such as surfactant-coated interfaces or even more complex systems such as the vicinity of a bilipidic membrane.[35,44] The simulated model was highly simplified, and we made no efforts to incorporate additional ingredients that might affect proton reactivity in a sensible fashion, such as the presence of additional ionic species (counterions and/or different charged headgroups) or the explicit consideration of quantum fluctuations originated in the lightness of the proton, to mention just a couple that we believe might be relevant. It should also be emphasized that in our model effects arising from polarization fluctuations in the force fields were not explicitly incorporated. Recent simulation studies show that the relative interfacial stability of simple ionic species at interfaces may change in a non-negligible fashion when these effects are incorporated.[4] Anyhow, we are confident that the results presented here remain physically sound and will be helpful in gaining new insights concerning fundamental reactive processes involving DIm and its derivatives in self-assembled structures.

Acknowledgment. J.R. and D.L. are staff members of CONICET (Argentina).

References and Notes

(1) A comprehensive description of recent advances in reactivity at water/air interfaces is presented in *Chem. Rev.* **2006**, *106*, Issue 4.

(2) Benjamin, I. *Acc. Chem. Res.* **1995**, *28*, 233; *Chem. Rev.* **1996**, *96*, 1449; *Annu. Rev. Phys. Chem.* **1997**, *48*, 407.

(3) Richmond, G. L. *Chem. Rev.* **2002**, *102*, 2693.

(4) Mucha, M.; Frigato, T.; Levering, L. M.; Allen, H. C.; Tobias, D. J.; Dang, L. X.; Jungwirth, P. *J. Phys. Chem. B* **2005**, *109*, 7617. Petersen, P. B.; Saykally, R. J.; Mucha, M.; Jungwirth, P. *J. Phys. Chem. B* **2005**, *109*, 10915.

(5) Gragson, D. E.; Richmond, G. L. *J. Am. Chem. Soc.* **1998**, *120*, 366.

(6) Zimdars, D. J.; Dadap, I.; Eisenthal, K. B.; Heinz, T. F. *Chem. Phys. Lett.* **1999**, *301*, 112. Zimdars, D.; Eisenthal, K. B. *J. Phys. Chem. A* **1999**, *103*, 10567. Zimdars, D.; Eisenthal, K. B. *J. Phys. Chem. B* **2001**, *105*, 3393. Pantano, D. A.; Laria, D. *J. Phys. Chem. B* **2003**, *107*, 297.

(7) Smart, J. L.; McCammon, J. A. *J. Am. Chem. Soc.* **1996**, *118*, 2283. Wang, H.; Zhao, X.; Eisenthal, K. B. *J. Phys. Chem. B* **2000**, *104*, 8855.

(8) Xiao, X.; Vogel, V.; Shen, Y. R.; Marowsky, G. *J. Chem. Phys.* **1991**, *94*, 2315.

(9) Benjamin, I.; Pohorille, A. *J. Chem. Phys.* **1993**, *98*, 236.

(10) Fitchett, B. D.; Conboy, J. C. *J. Phys. Chem. B* **2004**, *108*, 20255.

(11) Bowers, J.; Butts, C. P.; Martin, P. J.; Vergara-Gutierrez, M. C.; Heenan, R. K. *Langmuir* **2004**, *20*, 2191.

(12) de Duve, C.; de Barsy, T.; Poole, B.; Trouet, A.; Tulkens, P.; van Hoof, F. *Biochem. Pharmacol.* **1974**, *23*, 2495.

(13) Firestone, R. A.; Pisano, J. M. *J. Med. Chem.* **1979**, *22*, 1130.

(14) Miller, D. K.; Griggiths, E.; Lenard, J.; Firestone, R. A. *J. Cell Biol.* **1983**, *97*, 1841.

(15) Forster, S.; Scarlett, L.; Lloyd, J. B. *Biochem. Biophys. Acta* **1987**, *924*, 452.

(16) Boyer, M. J.; Horn, I.; Firestone, R. A.; Steele-Norwood, D.; Tannock, I. F. *Br. J. Cancer* **1993**, *67*, 81.

(17) Čuma, M.; Schmitt, U. W.; Voth, G. A. *Chem. Phys.* **2000**, *258*, 187.

(18) Čuma, M.; Schmitt, U. W.; Voth, G. A. *J. Phys. Chem. A* **2001**, *105*, 2814.

(19) Petersen, P. B.; Saykally, R. J. *J. Phys. Chem. B* **2005**, *109*, 7976.

(20) Tarbuck, T. L.; Ota S. T.; Richmond, G. L. *J. Am. Chem. Soc.* **2006**, *128*, 14519.

(21) Petersen, M. K.; Iyengar, S. S.; Day, T. J. F.; Voth, G. A. *J. Phys. Chem. B* **2004**, *108*, 14804.

(22) Wang, H. Second Harmonic Generation Studies at Liquid Interfaces. Ph.D. Thesis Defense Dissertation, Columbia University, New York, 1996; Chapter 3. An electronic version of this manuscript can be found at: http://digitalcommons.libraries.columbia.edu/dissertations/AAI9706914.

(23) Wang, H.; Zhao, X.; Eisenthal, K. B. *J. Phys. Chem. B* **2000**, *104*, 8855.

(24) Dang, X. L.; Pettitt, B. M. *J. Phys. Chem.* **1987**, *91*, 3349.

(25) Berendsen, H. J. C.; van der Spoel, D.; van Drunen, R. *Comput. Phys. Commun.* **1995**, *91*, 43. Lindahl, E.; Hess, B.; van der Spoel, D. *J. Mol. Model.* **2001**, *7*, 306. Schuettelkope, A. W.; van Aalten, D. M. F. *Acta Crystallogr.* **2004**, *D60*, 1355.

(26) Yeh, I.-C.; Berkowitz, M. L. *J. Chem. Phys.* **1999**, *111*, 3155.

(27) Åqvist, J.; Warshel, A. *Chem. Rev.* **1993**, *93*, 2523.

(28) Lobaugh, J.; Voth, G. A. *J. Chem. Phys.* **1996**, *104*, 2056. Schmitt, U. W.; Voth, G. A. *J. Phys. Chem. B* **1998**, *102*, 5547. Schmitt, U. W.; Voth, G. A. *J. Chem. Phys.* **1999**, *111*, 9361.

(29) Vuilleumier, R.; Borgis, D. *J. Phys. Chem. B* **1998**, *102*, 4261. Vuilleumier, R.; Borgis, D. *Chem. Phys. Lett.* **1998**, *284*, 71. Vuilleumier, R.; Borgis, D. *J. Chem. Phys.* **1999**, *111*, 4251.

(30) Laria, D.; Martí, J.; Guàrdia, E. *J. Am. Chem. Soc.* **2004**, *126*, 2125.

(31) A similar modification was operated in a recent study of proton transfer. See: Maupin, C. M.; Wong, K. F.; Soudackov, A. V.; Kim, S.; Voth, G. A. *J. Phys. Chem. A* **2006**, *110*, 631.

(32) Feynman, R. P. *Phys. Rev.* **1939**, *56*, 340.

(33) Lenarcik, B.; Ojczenasz, P. *J. Heterocycl. Chem.* **2002**, *39*, 287.

(34) For a detailed analysis of reaction coordinates for ion pair dissociation in solution, see: Geissler, P. L.; Dellago, C.; Chandler, D. *J. Phys. Chem. B* **1999**, *103*, 3706.

(35) Tepper, H. L.; Voth, G. A. *Biophys. J.* **2005**, *88*, 3095.

(36) Rodriguez, J.; Laria, D. *J. Phys. Chem. B* **2005**, *109*, 6473.

(37) Wilson, M. A.; Pohorille, A.; Pratt, L. R. *Chem. Phys. Lett.* **1989**, *129*, 209.

(38) Benjamin, I. *J. Chem. Phys.* **1991**, *95*, 3698.

(39) Pohorille, A.; Benjamin, I. *J. Chem. Phys.* **1991**, *94*, 5599.

(40) Torrie, G. M.; Valleau, J. P. *Chem. Phys. Lett.* **1974**, *28*, 578. Valleau, J. P.; Torrie, G. M. A guide for Monte Carlo for statistical mechanics. In *Statistical Mechanics, Part A*; Berne, B. J., Ed.; Plenum Press: New York, 1977; pp 169−194.

(41) Roux, B. *Comput. Phys. Commun.* **1995**, *91*, 275.

(42) Lapid, H.; Agmon, N.; Petersen, M. K.; Voth, G. A. *J. Chem. Phys.* **2005**, *122*, 14506.

(43) In order to bring the two sets of curves to the same asymptotic behavior at large distances, the density of site γ at the surface, that is, ρ_γ, was taken as half of the bulk value.

(44) For recent studies dealing for proton transfer in water in the close vicinity of a phospholipid membrane and in channels, see: Smondyrev, A. M.; Voth, G. A. *Biophys. J.* **2003**, *85*, 864. Wu, Y.; Voth, G. A. *Biophys. J.* **2002**, *82*, 1460. Xu, J.; Voth, G. A. *Proc. Natl. Acad. Sci. U.S.A.* **2005**, *102*, 6795.